UNIVERSITY OF LEEDS

This is a repository copy of *Two-way Quality Assessment Approach for Tumour Detection using Free-hand Strain Imaging*.

White Rose Research Online URL for this paper:
http://eprints.whiterose.ac.uk/101051/

Version: Accepted Version

Proceedings Paper:
Hyder, S, Harput, S orcid.org/0000-0003-0491-4064, Alomari, Z et al. (1 more author) (2014) Two-way Quality Assessment Approach for Tumour Detection using Free-hand Strain Imaging. In: 2014 IEEE International Ultrasonics Symposium Proceedings. IUS, 03-06 Sep 2014, Chicago, IL, USA. IEEE , pp. 1853-1856. ISBN 978-1-4799-7049-0

https://doi.org/10.1109/ULTSYM.2014.0460

© 2014 IEEE. This is an author produced version of a paper published in 2014 IEEE International Ultrasonics Symposium Proceedings. Personal use of this material is permitted. Permission from IEEE must be obtained for all other uses, in any current or future media, including reprinting/republishing this material for advertising or promotional purposes, creating new collective works, for resale or redistribution to servers or lists, or reuse of any copyrighted component of this work in other works. Uploaded in accordance with the publisher's self-archiving policy.

Reuse
Unless indicated otherwise, fulltext items are protected by copyright with all rights reserved. The copyright exception in section 29 of the Copyright, Designs and Patents Act 1988 allows the making of a single copy solely for the purpose of non-commercial research or private study within the limits of fair dealing. The publisher or other rights-holder may allow further reproduction and re-use of this version - refer to the White Rose Research Online record for this item. Where records identify the publisher as the copyright holder, users can verify any specific terms of use on the publisher's website.

Takedown
If you consider content in White Rose Research Online to be in breach of UK law, please notify us by emailing eprints@whiterose.ac.uk including the URL of the record and the reason for the withdrawal request.

White Rose university consortium
Universities of Leeds, Sheffield & York

eprints@whiterose.ac.uk
https://eprints.whiterose.ac.uk/

Two-way Quality Assessment Approach for Tumour Detection using Free-hand Strain Imaging

Safeer Hyder, Sevan Harput, Zainab Alomari and Steven Freear
Ultrasound Group, School of Electronic and Electrical Engineering, University of Leeds, UK.
Email: el10shl@leeds.ac.uk

***Abstract*—A novel two-way image quality assessment method is proposed for free-hand strain imaging. In elasticity imaging, tissue with different stiffness exhibit varying contrast in the strain images and detectability of a lesion is measured using elastographic contrast-to-noise ratio (CNR_e). Representing quality of strain images quantitatively is vital for improving imaging techniques and also for clinical diagnosis. It avoids the subjective approach of interpreting strain images. Conventionally, contrast between stiff lesion and surrounding soft tissue is measured using contrast-to-noise ratio and strain image with the highest CNR_e amplitude is considered an optimal strain image. However experimental results have suggested that merely CNR_e metric is often misleading and does not always represent the true elastic modulus contrast as the correlation coefficient falls below an acceptable levels and accuracy is compromised. Therefore in this study, the objective is to propose a comprehensive strain image quality assessment method which is reliable for clinical examinations and research.**

I. Introduction

Elastography is based on the premise that various pathologies such as cancer change the elasticity of tissues and develop the diagnostic information in terms of elastic modulus (E). By comparison, conventional B-mode imaging visualizes anatomical features using acoustic impedance (Z) difference and is unable to image elasticity changes in the tissues [1].

Elasticity imaging falls into two major categories: the first category of techniques measure the strain when soft tissue is deformed externally or internally while the second category of techniques are based on shear wave generation and followed by quantitatively measuring elastic modulus in Pascal (Pa) using shear wave speed. Free-hand strain imaging belongs to the first category and is preferred due to its simple implementation on the existing B-mode ultrasound system [2], [3]. In this approach, ultrasound echo radio frequency (RF) data is acquired after multiple compression and relaxation stages, followed by processing the successive RF data scan lines using speckle tracking algorithms. The computed local strain values are displayed using a jet colourmap and underlying varying strain contrast is visualized using different colours [4].

The quality of the strain image is measured using the elastographic signal-to-noise ratio (SNR_e), elastographic contrast-to-noise ratio (CNR_e) and spatial resolution metrics. For heterogeneous tissue, lesion detectability of the tumour is assessed by measuring image contrast CNR_e between the tumour and surrounding tissues. Improvement in the elastographic signal-to-noise ratio (SNR_e) directly improves the elastographic contrast-to-noise ratio (CNR_e) keeping spatial resolution constant [5].

Conventionally in the research literature, while characterizing the performance of the strain images for lesion detectability only CNR_e is used as a quality metric and strain images with higher values are regarded as optimal strain image [6], [7]. Although, the strain contrast generated during deformation of the soft tissue results from complex interaction between the elastic profile of the tissue, tumour's shape, size, location, and boundary conditions [8]. Optimal elastogram selection based on merely CNR_e is often misleading because higher contrast does not guarantee accurate estimation as the correlation coefficient falls below the significant level ($\rho < 0.7$) due to the decorrelation noise and diagnostic accuracy is compromised.

For medical use, in order to improve the diagnostic confidence of the strain imaging technique, strain images need to be as accurate and reliable as possible. This requirement necessitates another quality metric along with CNR_e which increases the diagnostic accuracy and helps to scrutinize the optimal strain image. In this study, a novel metric based on correlation coefficient named the noise masked area (NMA) percentage is introduced along with CNR_e. The NMA percentage calculates and locates the area of the strain image where strain calculation correlation coefficient (ρ) falls below a significant level ($\rho < 0.7$).

This two-way method for strain image quality assessment of the strain images is proposed to enhance the strain estimation accuracy and diagnostic performance of the technique. Two phantoms with different sized lesions are prepared, results are produced, the method is applied and the optimal strain image is selected.

II. Methodology

In order to calculate the image quality of strain images, region-of-interest (ROI) R2 inside the tumour and two other ROI R1 and R3 are selected outside the tumour as schematically depicted in the Fig. 1. The size of the ROI is 5 x 5 mm and 3 x 3 mm for 10-mm and 5-mm inclusion phantom respectively [9].

In the first step, normalized elastographic contrast-to-noise ratio (CNR_e) between lesion and background is calculated using equation 1. The contrast is calculated between regions 1 and 2, and between 3 and 2 separately, then both the contrast values are averaged and finally normalized. All the normalized CNR_e values which are greater than the 0.7 threshold level are regarded as possessing the significant level of CNR_e and are

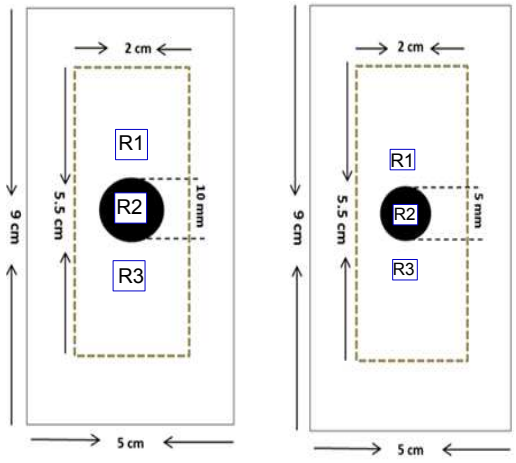

Fig. 1. Tissue mimicking phantom geometry with 10-mm (left) and 5-mm lesion (right). The rectangles in each denote region-of-interst; R1, R2, and R3 used to calculate elastographic contrast-to-noise ratio between lesion and background. The dimensions of region-of-interest are 5 mm x 5 mm and 3 mm x 3 mm for 10 mm and 5 mm lesion, respectively.

selected for the second step. In the second step, noise-masked-area (NMA) percentage is calculated using equation 2 for all the selected images and the least noisy elastogram is selected as the optimal elastogram. For clinical diagnostic use, only strain image with the optimal quality is displayed with the noise-masked version, which helps to locate noisy portions of the finally selected strain image.

$$CNR_e = \frac{2(\bar{s}_l - \bar{s}_b)}{std_l + std_b} \tag{1}$$

$$NMA(\%) = \frac{\rho < 0.7}{total\ \rho} \times 100 \tag{2}$$

The $\bar{s}_l$ and $\bar{s}_b$ are mean strain for lesion and background, while std_l and std_b are strain standard deviation for lesion and background portions respectively and ρ denotes correlation coefficient obtained by normalized cross correlation [10].

III. Experimental Setup

Two agar-gelatin tissue-mimicking phantoms with lesions three times stiffer than the background were prepared with lesion size of 10-mm and 5-mm respectively. A similar percentage of gelatin (*Science Lab, Inc*) is maintained in both background and stiffer inclusion part to avoid change in the size and shape of the inclusion due to osmosis. The amount of agar (*Science Lab, Inc*) determines the stiffness in the phantom, therefore the agar portion in the inclusion is three times higher than the background. Solid soda-lime glass beads (*mo.sci, corp*) with an average diameter of 20 μm are added to produce scattering and attenuation properties [11].

A L3-8/40EP medical ultrasound traducer with 128 element is excited by a Gaussian pulse with 6-dB bandwidth of 5 MHz, centred at 5.5 MHz driven by a custom-built Ultrasound Array Research Platform (UARP) developed by the ultrasound group [12], [13]. The imaging depth and focal depth of the experiment are set to 75 mm and 55 mm respectively. The fifty six scan lines are acquired for each RF image with aperture size of 9.6 mm having 32 elements, which spans 20 mm in the lateral direction using linear array imaging.

TABLE I
Imaging and Signal Processing Parameters

Parameter	Value
Sampling frequency	50 MHz
Bandwidth (BW)	5 MHz
Centre Frequency (f_c)	5.5 MHz
Acoustic speed in phantom (c)	1500 m/s
Imaging depth	75 mm
Correlation Window length (T)	4 mm
Correlation window separation (ΔT)	0.5 mm

The tissue mimicking phantoms were compressed up to 3.56% with an increment of 0.22% using the medical probe and a total of 17 RF frames are acquired . The axial strain was estimated by a normalized cross-correlation algorithm with adaptive temporal stretching [10]. The correlation window length (T) and correlation window separation (ΔT) were set to 4 mm and 0.5 mm respectively, keeping the correlation window less than the lesion diameter [5]. The diagram of the experimental set up is depicted in the Fig. 2.

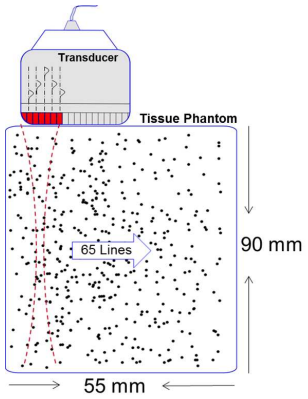

Fig. 2. Tissue mimicking phantom is compressed using the medical probe with interval of 0.22% and RF data is acquired using linear array imaging. The focal point is set at the middle of the phantom where lesion is located, and 65 scan lines are acquired to scan 20 mm lateral imaging dimension.

IV. Results and Discussion

The quality assessment parameters used to examine the lesion contrast and estimation accuracy are presented in Fig 3 and Fig. 4 for 10-mm and 5-mm lesion respectively. The image CNR_e between the lesion portion and the surrounding portion is plotted for each applied strain. In the second row of each figure, the noise masked area of the elastogram is calculated and plotted.

For 10-mm lesion phantom, three ROI are selected each having dimensions of 5 mm x 5 mm. The first ROI is above

the lesion, one inside the lesion, and one beneath the lesion. The size of the ROI is chosen according to the diameter of the lesion. The strain contrast between the lesion and the background is calculated, in order to cover both above and below the lesion portions, CNR_e is calculated between region-I and region-II and in a similar way between region-III and region-II. At the end, these two contrast ratios are averaged and normalized.

It can be observed for the 10-mm phantom, the CNR_e improves as the applied strain increases and deteriorates for strain values higher than the 1.56% as shown in Fig. 3. For the 5-mm phantom, peak CNR_e is achieved when the applied strain is 1.78% and then degrades. This bandpass response of the CNR_e for applied strain is consistent with the strain filter concept of strain imaging [14]. Pointing to Fig. 3, first two strain values do not produce enough contrast to reach the threshold level, but when the applied strain is increased from 0.67% to 2.22% the strain contrast falls into the significant contrast window. Again, for the strain values higher than the 2.44%, the strain falls below the threshold line. In this scenario, first two and final six strain images can be discarded because of poor strain contrast. There are 8 and 5 CNR_e values for 10-mm phantom and 5-mm phantom respectively, which are above the threshold level which is proposed as a minimum requirement of CNR_e.

To select which strain image is reliable for clinical use the noised-masked area index is used to guarantee that strain estimation has significant accuracy. The NMA percentage degrades directly with applied strain due to decorrelation noise as shown in Fig. 3 and Fig. 4. For 10-mm phantom, when strain image obtains peak CNR_e at 1.56%, noisy area is 44% , therefore, out of 8 significant CNR_e strain images, the strain image which has minimum noisy area with strain 0.67% is selected as an optimal strain image. Similarly for the 5-mm phantom, out of 5 CNR_e values which are above the CNR_e threshold level, 0.89% strain image is having least noisy portion.

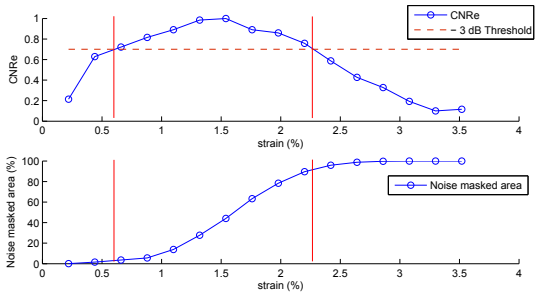

Fig. 3. Normalized CNR_e and noise masked area (NMA) percentage plots of the tissue mimicking phantom with 10-mm lesion. The marker positions indicate CNR_e values and dashed red line indicates threshold line of significant normalized CNR_e (0.7). There are 8 applied strain values obtaining significant values of the normalized CNR_e. In the second row, using NMA metric strain image with strain of 0.67% has least noisy portion.

For both phantoms, strain images are produced for all the 16

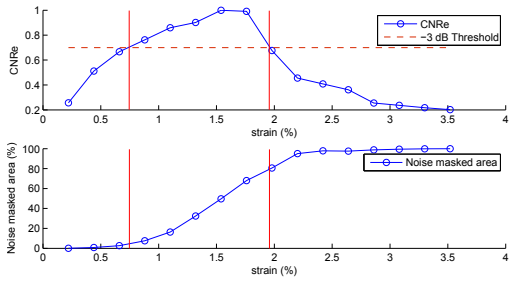

Fig. 4. Normalized CNR_e and noise masked area (NMA) percentage plots of the tissue mimicking phantom with 5-mm lesion. The marker positions indicate CNR_e values and dashed red line indicates threshold line of significant normalized CNR_e (0.7). There are 5 applied strain values obtained significant values of the normalized CNR_e. In the second row, using NMA metric strain image with strain of 0.89% has least noisy portion.

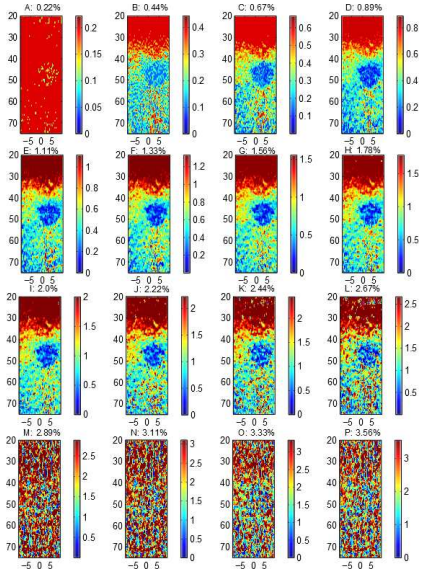

Fig. 5. The strain images for the phantom with 10-mm lesion. The strain images for the all sixteen strain values are in the ascending order from left to right and top to bottom. The strain applied is indicated at the top of the each strain image. The strain images from C to J are found within the -3 dB threshold of maximum contrast. Out of these 8 strain images, one strain image which has least noised-masked portion is selected (C i.e 0.67%) as the optimal strain image.

applied strain values from 0.22% to 3.56% labelled A to P and displayed using jet colourmap which ranges from blue to red [15] as shown in Fig. 5 and Fig. 6. The colorbar indicates the range of estimated strain while applied strain value is shown at the top of the each image. It can be observed that, lesions are clearly visible in the strain images both in the 10-mm and 5-mm phantom for 0.67% to 2.22% (C to J) and for 0.89% to 1.78% (C to I) respectively. It can also be observed that, strain imaging maintains a significant contrast for large values of strain (i.e 8) for 10-mm lesion phantom while for 5-mm lesion phantom only 5 values of strain are able to obtain the significant contrast. From this phenomenon it can be inferred

that, dynamic range of the strain which produce significant contrast degrades with lesion size.

These strain images obtain the significant level of contrast and visually there is little difference in the quality, therefore a further NMA metric is used to find out the optimal strain image. Out of these images, strain image 0.67% (C) for 10-mm phantom which has noisy portion of 3.54% and strain image 0.89% (D) for 5-mm phantom which has a noisy portion of 7.52% is selected as the optimal strain image. Finally as selected strain images are not absolutely noise free but they have least portions of noise and these portions are masked by the white mask to locate those portions as shown in Fig. 7.

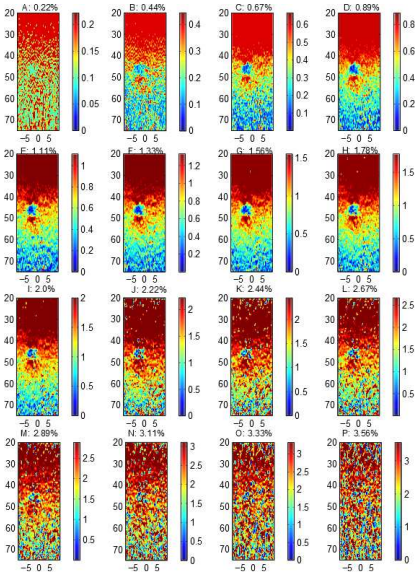

Fig. 6. The strain images for the phantom with 5-mm lesion. The strain images for the all sixteen strain values are in the ascending order from left to right and top to bottom. The strain applied is indicated at the top of the each strain image. The strain images from D to H are found within the -3 dB threshold of maximum contrast. Out of these 5 strain images, one strain image which has least noised-masked portion is selected (D i.e 0.89%) as the optimal strain image.

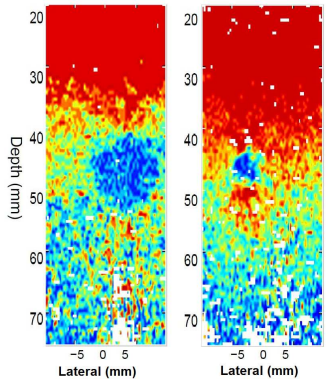

Fig. 7. Optimal maksed strain images for 10-mm phantom (left) and 5-mm phantom (right). Portions of white mask indicates points in the strain image which are considered noisy.

V. Conclusions

Conventionally, the interpretation of strain images is based on the contrast ratios, while other factors which define the accuracy of the estimation such as correlation coefficient are usually ignored. Here, a two-way approach is presented to make sure the final selected strain image for the tumour detection and localization possesses significant contrast without compromising the estimation accuracy. The presented method can provide a significant basis for the optimization of the free-hand strain imaging and enhancing the clinical diagnostic confidence on the imaging technique.

References

[1] P. N. Wells and H.-D. Liang, "Medical ultrasound: imaging of soft tissue strain and elasticity," *Journal of The Royal Society Interface*, vol. 8, no. 64, pp. 1521–1549, 2011.

[2] J. Ophir, I. Cspedes, H. Ponnekanti, Y. Yazdi, and X. Li, "Elastography: A quantitative method for imaging the elasticity of biological tissues," *Ultrasonic Imaging*, vol. 13, no. 2, pp. 111 – 134, 1991.

[3] K. R. Nightingale, P. J. Kornguth, W. F. Walker, B. A. McDermott, and G. E. Trahey, "A novel ultrasonic technique for differentiating cysts from solid lesions: Preliminary results in the breast," *Ultrasound in Medicine & Biology*, vol. 21, no. 6, pp. 745 – 751, 1995.

[4] S. Park, S. R. Aglyamov, W. G. Scott, and S. Y. Emelianov, "Strain imaging using conventional and ultrafast ultrasound imaging: Numerical analysis," *Ultrasonics, Ferroelectrics and Frequency Control, IEEE Transactions on*, vol. 54, no. 5, pp. 987–995, 2007.

[5] S. Srinivasan, J. Ophir, and S. Alam, "Theoretical derivation of snr, cnr and spatial resolution for a local adaptive strain estimator for elastography," *Ultrasound in medicine & biology*, vol. 30, no. 9, pp. 1185–1197, 2004.

[6] H. Peng and D. C. Liu, "Enhanced ultrasound strain imaging using chirp-coded pulse excitation," *Biomedical Signal Processing and Control*, vol. 8, no. 2, pp. 130 – 141, 2013.

[7] J. Liu and M. F. Insana, "Coded pulse excitation for ultrasonic strain imaging," *Ultrasonics, Ferroelectrics and Frequency Control, IEEE Transactions on*, vol. 52, no. 2, pp. 231–240, 2005.

[8] M. Bilgen, "Target detectability in acoustic elastography," *Ultrasonics, Ferroelectrics and Frequency Control, IEEE Transactions on*, vol. 46, no. 5, pp. 1128–1133, 1999.

[9] S. Park, S. R. Aglyamov, and S. Y. Emelianov, "Elasticity imaging using conventional and high-frame rate ultrasound imaging: Experimental study," *Ultrasonics, Ferroelectrics and Frequency Control, IEEE Transactions on*, vol. 54, no. 11, pp. 2246–2256, 2007.

[10] S. K. Alam, J. Ophir, and E. E. Konofagou, "An adaptive strain estimator for elastography," *Ultrasonics, Ferroelectrics and Frequency Control, IEEE Transactions on*, vol. 45, no. 2, pp. 461–472, 1998.

[11] E. L. Madsen, M. A. Hobson, H. Shi, T. Varghese, and G. R. Frank, "Tissue-mimicking agar/gelatin materials for use in heterogeneous elastography phantoms," *Physics in medicine and biology*, vol. 50, no. 23, p. 5597, 2005.

[12] P. R. Smith, D. M. Cowell, B. Raiton, C. V. Ky, and S. Freear, "Ultrasound array transmitter architecture with high timing resolution using embedded phase-locked loops," *Ultrasonics, Ferroelectrics and Frequency Control, IEEE Transactions on*, vol. 59, no. 1, pp. 40–49, 2012.

[13] S. Harput, M. Arif, J. McLaughlan, D. M. Cowell, and S. Freear, "The effect of amplitude modulation on subharmonic imaging with chirp excitation," *Ultrasonics, Ferroelectrics and Frequency Control, IEEE Transactions on*, vol. 60, no. 12, pp. 2532–2544, 2013.

[14] T. Varghese and J. Ophir, "A theoretical framework for performance characterization of elastography: the strain filter," *Ultrasonics, Ferroelectrics and Frequency Control, IEEE Transactions on*, vol. 44, no. 1, pp. 164–172, 1997.

[15] K. M. Hiltawsky, M. Krüger, C. Starke, L. Heuser, H. Ermert, and A. Jensen, "Freehand ultrasound elastography of breast lesions: clinical results," *Ultrasound in medicine & biology*, vol. 27, no. 11, pp. 1461–1469, 2001.